Layered Lithium Vanadium Fluorophosphate, $Li_5V(PO_4)_2F_2$: A 4 V Class Positive Electrode Material for Lithium-Ion Batteries

Y. Makimura,[†] L. S. Cahill,[‡] Y. Iriyama,[†,§] G. R. Goward,*[,‡] and L. F. Nazar*[,†]

Department of Chemistry, University of Waterloo, Waterloo, Ontario, Canada, Department of Chemistry, McMaster University, Hamilton, Ontario, Canada, and Department of Energy and Hydrocarbon Chemistry, Kyoto University, Kyoto, Japan

Received August 18, 2007. Revised Manuscript Received March 11, 2008

A single-phase, well-crystallized $Li_5V(PO_4)_2F_2$/carbon nanocomposite has been prepared by an optimized solid-state route, and its electrochemical behavior was examined as a positive electrode active material in lithium-ion batteries. The microcrystalline powder was synthesized by the reaction of amorphous VPO_4/C with Li_3PO_4 and LiF. Synthesis of the VPO_4/C precursor utilized carbon to reduce V_2O_5 and simultaneously create a nanoparticle reactive material, with the amount being tailored to result in a small excess at the end of the reaction to increase the bulk electronic conductivity of the final $Li_5V(PO_4)_2F_2$ composite. Quench techniques were used to isolate the metastable two-dimensional $Li_5V(PO_4)_2F_2$ as a pure single phase. ^{6}Li MAS NMR studies identified the crystallographic lithium sites and provided information on lithium-ion mobility and exchange in the two-dimensional layered structure. Lithium cells of the $Li_5V(PO_4)_2F_2$/C composite exhibited a reversible plateau at 4.15 V followed by a second plateau at 4.65 V, which correspond to the V^{3+}/V^{4+} and V^{4+}/V^{5+} redox couples, respectively, and a charge capacity of 165 mA h g^{-1}, which is close to theoretical (170 mA h g^{-1}). These operating voltages are very similar to those of the V^{3+}/V^{4+} couple in $Li_3V_2(PO_4)_3$ or $LiVPO_4F$ and the V^{4+}/V^{5+} couple in $Li_3V_2(PO_4)_3$.

Introduction

Lithium insertion materials based on lithium transition metal oxides have been extensively examined and modified to a quite high level.[1–4] They exhibit an average operating voltage of around 4 V and are used as positive electrode active materials for practical lithium-ion batteries. These oxides based on $LiMO_2$ (M = Co, Mn, Ni, Al) typically possess an $R\bar{3}m$ structure composed of cubic close packed oxygen layers, with M or Li occupying octahedral sites in alternate sheets to form a layered structure. Facile 2D lithium-ion conduction paths and good ion diffusion properties hence result. However, lithium insertion materials are not limited to oxides if one can create these ideal structural properties in other compounds. Lithium transition metal phosphates were first proposed as positive electrodes many years ago,[5,6] and recent research has clearly demonstrated the promise and viability of this class of lithium insertion materials. They exhibit voltages about 1.5−2.0 V higher than the corresponding oxides due to the so-called inductive effect.[7] The best known member of the family, $LiFePO_4$, operates at 3.5 V, and numerous other phosphates display even higher redox potentials.[8–11] Recently, lithium metal fluorophosphates, which have their analogues in the mineral world as hydroxyphosphates, have also been examined as positive electrodes. Barker et al. first reported $LiVPO_4F$, which is isostructural with tavorite, i.e., $LiFePO_4OH$, and exhibits a flat voltage profile at 4 V.[12]

In our previous paper,[13] we reported a new material, $Li_5V(PO_4)_2F_2$, with a two-dimensional layered structure. Along with finding the way to grow single crystals of the material, whose synthesis is complicated by metastability (with respect to $Li_3V_2(PO_4)_3$), we described preliminary electrochemistry results on bulk microcrystalline powders. For the latter, we employed two routes:

$$Li_3V_2(PO_4)_3 + Li_3PO_4 + 4LiF \rightarrow 2Li_5V(PO_4)_2F_2 \quad (1)$$

$$VPO_4 + Li_3PO_4 + 2LiF \rightarrow Li_5V(PO_4)_2F_2 \quad (2)$$

Because the $Li_3V_2(PO_4)_3$ precursor resulted in large amounts of Li_3PO_4 and V_2O_3 impurities in addition to the majority target phase, we focused on route 2 to prepare a single $Li_5V(PO_4)_2F_2$ microcrystalline powder. In this paper, we

* Corresponding author. E-mail: lfnazar@uwaterloo.ca (L.F.N.); goward@mcmaster.ca (G.R.G.).
[†] University of Waterloo.
[‡] McMaster University.
[§] Kyoto University.

(1) Ohzuku, T.; Ueda, A. *Solid State Ionics* **1994**, *69*, 201.
(2) Delmas, C.; Ménétrier, M.; Croguennec, L.; Saadoune, I.; Rougier, A.; Pouillerie, C.; Prado, G.; Grüne, M.; Fournès, L. *Electrochim. Acta* **1999**, *45*, 243.
(3) Ammundsen, B.; Paulsen, J. *Adv. Mater.* **2001**, *13*, 943.
(4) Whittingham, M. S. *Chem. Rev.* **2004**, *104*, 4271.
(5) Padhi, A. K.; Nanjudaswamy, K. S.; Goodenough, J. B. *J. Electrochem. Soc.* **1997**, *144*, 1188.
(6) Delmas, C.; Nadiri, A.; Soubeyroux, J. L. *Solid State Ionics* **1988**, *28−30*, 419.
(7) Padhi, A. K.; Nanjudaswamy, K. S.; Masquelier, C.; Goodenough, J. B. *J. Electrochem. Soc.* **1997**, *144*, 2581.
(8) Li, G.; Azuma, H.; Tohda, M. *Electrochem. Solid-State Lett.* **2002**, *5*, A135.
(9) Amine, K.; Yasuda, H.; Yamachi, M. *Electrochem. Solid-State Lett.* **2000**, *3*, 178.
(10) Kerr, T. A.; Gaubicher, J.; Nazar, L. F. *Electrochem. Solid-State Lett.* **2000**, *3*, 460.
(11) Yin, S.-C.; Grondey, H.; Strobel, P.; Anne, M.; Nazar, L. F. *J. Am. Chem. Soc.* **2003**, *125*, 326.
(12) Barker, J.; Saidi, M. Y.; Swoyer, J. L. *J. Electrochem. Soc.* **2003**, *150*, A1394.
(13) Yin, S.-C.; Subramanya Herle, P.; Higgins, A.; Taylor, N. J.; Makimura, Y.; Nazar, L. F. *Chem. Mater.* **2006**, *18*, 1745.

10.1021/cm702346n CCC: $40.75
Published on Web 06/14/2008

describe the detailed synthesis process to produce bulk $Li_5V(PO_4)_2F_2$ together with its carbon composite and discuss its electrochemical behavior in lithium cells. Li-ion exchange and mobility are probed in the material by ^{6}Li MAS NMR studies.

Experimental Section

A single well-crystallized VPO_4 powder was prepared by heating a stoichiometric mixture of NH_4VO_3 and $(NH_4)_2HPO_4$ at 350 °C for 2 h followed by 3 h at 900 °C under a H_2/N_2 (7%) mixed gas flow. The VPO_4/carbon (C) composite was prepared by a carbothermal reduction method using carbon black as a reducing agent.[14] A stoichiometric mixture of V_2O_5 and $(NH_4)_2HPO_4$ with a 0.5 M excess of carbon black was ball-milled for 30 min, pressed into pellet, and then heated at several different temperatures for 4 h under a H_2/N_2 (7%) mixed gas flow. $Li_5V(PO_4)_2F_2$ or its carbon composite was synthesized from VPO_4 mixed with Li_3PO_4 and LiF, using a stoichiometric excess amount of LiF as a flux. For the quench synthesis, the above mixture was placed in a sealed stainless-steel tube filled with Ar. The stainless-steel tube was inserted in a tube furnace set to various temperatures. After 1 h, the tube was quenched by quickly immersing it in a cold bath. Processing methods are further described in the Results and Discussion section. ^{6}Li enriched samples were prepared similarly, using pure $^6Li_3PO_4$ as the reagent, and ^{7}LiF as the reagent/flux. Because VPO_4 and $Li_5V(PO_4)_2F_2$ dissolve in HF, the amount of carbon in VPO_4/C or the $Li_5V(PO_4)_2F_2$/C composite was determined by stirring the composite in 1 M HF aqueous solution for 48 h.

Samples were characterized by powder X-ray diffraction using a Bruker D8 Advance powder diffractometer in standard Bragg−Brentano geometry and Cu Kα radiation (λ = 1.54046Å). The electrochemical properties of $Li_5V(PO_4)_2F_2$ were examined by using Swagelok-type cells, in which the positive electrode consisted of 88 wt % $Li_5V(PO_4)_2F_2$/C composite, 6 wt % Super S carbon, and 6 wt % polyvinylidene fluoride (PVdF) binder. The negative electrode was lithium foil supported on a current collector. The two electrodes were separated by a glass fiber sheet immersed in 1 M $LiPF_6$ in ethylene carbonate (EC)/dimethyl carbonate (DMC) solution (1/1 by volume). The cells were operated in galvanostatic mode using a Macpile controller.

^{6}Li and ^{7}Li MAS NMR spectra were acquired at Larmor frequencies of 44.1 and 116.6 MHz, respectively, on a Bruker AV-300 spectrometer. All experiments were carried out at room temperature using a custom probe fitted to support 1.8 mm diameter rotors, spinning at frequencies up to 40 kHz. The spectra are referenced to 1 M LiCl (aq) (0 ppm). Both ^{6}Li and ^{7}Li NMR spectra were acquired using a 90° pulse length of 2.5 μs and a recycle delay of 50 ms. ^{6}Li spectral decompositions were performed using the xedplot program in the Bruker XwinNMR software. This allows variation of peak position, peak height, line width and the ratio of Gaussian to Lorentzian functions. 100% Gaussian lineshapes were used, as this simplifies the comparison of relative intensities. 2D exchange spectra were acquired using mixing times between 1 μs and 7 ms. The longer mixing time of 7 ms is limited by the spin−lattice relaxation time (T_1) of the resonances; after this time, the signal at higher frequency completely decays. The number of slices in the indirect dimension was 10 240, with 128 transients averaged per slice. The increment for the slices in the indirect dimension is 1 μs, which is the limit for the spectrometer. A Gaussian broadening value of 0.0005 was used for the mixing time of 7 ms. To resolve $Li3_E$, we applied a broadening value of 0.01 (for spectra with mixing times of 1 ms and 1 μs). Phase-sensitive detection in t_1 was achieved through use of States-TPPI.

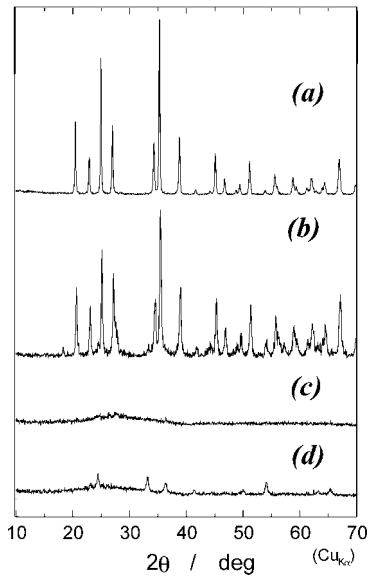

Figure 1. (a) XRD pattern of a single well-crystallized VPO_4 powder prepared by heating a stoichiometric mixture of NH_4VO_3 and $(NH_4)_2HPO_4$ at 350 °C for 2 h followed by 900 °C for 3 h under a H_2/N_2 (7%) mixed gas flow; (b−d) VPO_4/C composites prepared by a carbothermal reduction method using a stoichiometric mixture of V_2O_5 and $(NH_4)_2HPO_4$ with a 0.5 M excess of carbon black heated at (b) 800, (c) 700, or (d) 600 °C for 4 h under a H_2/N_2 (7%) mixed gas flow.

Results and Discussion

Synthesis. *Preparation of VPO_4 and Its Carbon Composite.* Figure 1a shows the XRD pattern of a well-crystallized VPO_4 powder produced from NH_4VO_3 and $(NH_4)_2HPO_4$ by optimizing the preparation method. Although we tried to tune the synthesis process to use this material as a precursor for $Li_5V(PO_4)_2F_2$, impurities of Li_3PO_4, V_2O_3, and $Li_3V_2(PO_4)_3$ always resulted in the reaction products. We found that nanocrystalline VPO_4 was much more reactive owing to its small particle size (<40 nm as determined by SEM) and higher surface area. It was prepared via a carbothermal reduction method that reduces V_2O_5 to V^{III} in the presence of phosphate. This method is well-known as a route to prepare transition metal compounds starting from those in higher oxidation states. Carbon black mixed with the desired starting materials is used as a reducing agent during the synthesis process, and any residual carbon can function as a conductive additive in the product. Barker et al. recently used this method to prepare lithium transition metal phosphates and fluorophosphates.[15,12,16] Figure 1 also shows XRD patterns of VPO_4/C composites prepared at several temperatures. When the reaction mixture of V_2O_5 and $(NH_4)_2HPO_4$ with carbon black (0.5 M excess) was heated at 800 °C, the XRD pattern obtained was that of crystallized VPO_4 (Figure 1b); conversely heating at less than 600 °C resulted in impurities of V_2O_3, VO_2, and other vanadium oxides in the

(14) *Handbook of Preparative Inorganic Chemistry*; Brauer, G., Ed.; Academic Press: New York, 1963.

(15) Barker, J.; Saidi, M. Y.; Swoyer, J. L. *J. Electrochem. Soc.* **2003**, *150*, A684.

(16) Barker, J.; Saidi, M. Y.; Swoyer, J. L. *Electrochem. Solid-State Lett.* **2003**, *6*, A53.

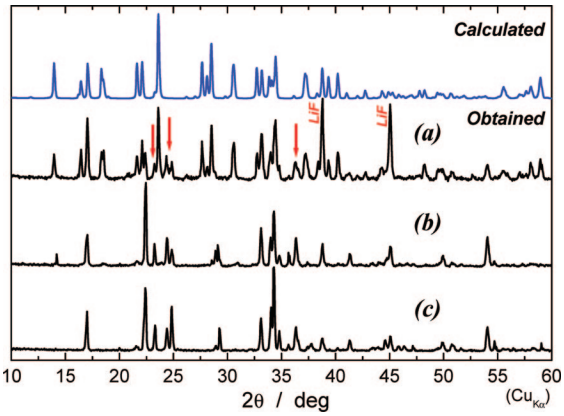

Figure 2. XRD patterns of the reaction products prepared by heating a mixture of amorphous VPO_4/C composite, Li_3PO_4, and LiF at 800 °C under a H_2/N_2 (7%) mixed gas flow for (a) ≤1, (b) 3, or (c) 15 h. A 3 M excess amount of LiF was used as a flux. The calculated XRD pattern of $Li_5V(PO_4)_2F_2$ is also shown for comparison. XRD peaks highlighted by arrows in (a) indicate impurity phases of Li_3PO_4, V_2O_3, and $Li_3V_2(PO_4)_3$.

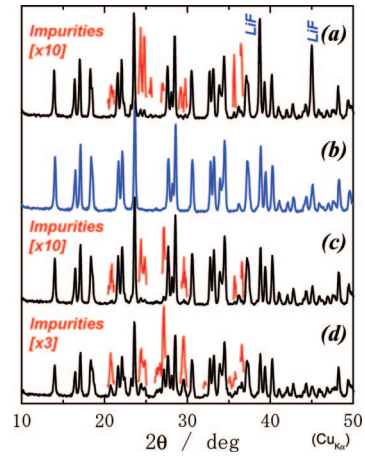

Figure 3. XRD patterns of $Li_5V(PO_4)_2F_2$/C composite prepared by heating a mixture of amorphous VPO_4/C composite, Li_3PO_4, and LiF at 700 °C for 1 h, followed by quench-cooling to room temperature. An excess amount of LiF was used as a flux: (a) 3, (b) 1, or (c) 0.5 M excess, or (d) stoichiometric amount. XRD peaks of impurity phases are expanded (a) 10, (c) 10, and (d) 3 times and shown in red at the same locations.

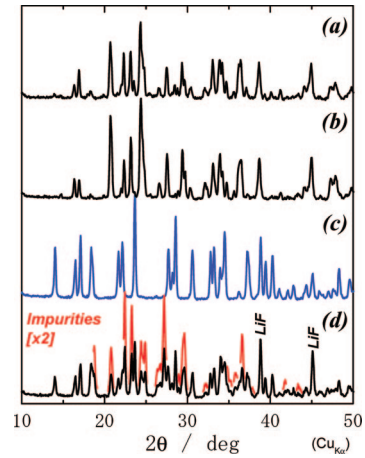

Figure 4. XRD patterns of $Li_5V(PO_4)_2F_2$/C composite prepared by heating a mixture of amorphous VPO_4/C composite, Li_3PO_4, and LiF at (a) 900, (b) 800, (c) 700, or (d) 600 °C for 1 h, followed by quick-cooling to room temperature. A 1 M excess amount of LiF was used as a flux. XRD peaks of impurity phases are expanded in (d) twice and shown in red at the same locations. XRD patterns in (a) and (b) correspond to that of $Li_3V_2(PO_4)_3$.

products (Figure 1d). Figure 1c shows that the reaction product heated at 700 °C for 3−4 h was a "pure" poorly crystalline VPO_4/carbon composite. The carbon content was ~20 wt % as determined from gravimetric analysis.

Formation of $Li_5V(PO_4)_2F_2$. Figure 2 shows our first attempts to prepare $Li_5V(PO_4)_2F_2$/C by reacting the amorphous VPO_4/C composite with an excess amount of LiF. The latter serves as both reactant and flux. As shown in Figure 2c, the reaction product heated at 800 °C for 15 h was a mixture of Li_3PO_4, LiF, and V_2O_3. A shorter heating time of 3 h at 800 °C also gave a mixture of Li_3PO_4, LiF, and V_2O_3, with a trace of $Li_5V(PO_4)_2F_2$ as shown in Figure 2b. Figure 2a displays the XRD pattern of the reaction product heated at 800 °C for less than 1 h. Diffraction peaks corresponding to $Li_5V(PO_4)_2F_2$ were evident under these conditions, although some impurity phases are still seen. These results indicate that $Li_5V(PO_4)_2F_2$ forms quickly but is then decomposed into Li_3PO_4, LiF, and V_2O_3 on heating because of its metastability. We also noted that other methods to coat the particles with carbon precursors such as resorcinol-formaldehyde carbon gel resulted in unacceptable levels of impurities.

The above trials suggested that rapid heating and quenching are necessary to produce $Li_5V(PO_4)_2F_2$ as a single-phase powder. Synthesis was performed in sealed stainless steel tubes as described in the experimental section. To fine-tune the preparation of this metastable phase, the temperature and excess amount of LiF were adjusted until optimum results were achieved. Figure 3 shows the XRD patterns of the samples prepared at 700 °C by varying the LiF ratio. As shown in Figure 3d, a stoichiometric amount of LiF resulted in a material with many impurities of Li_3PO_4, V_2O_3, and $Li_3V_2(PO_4)_3$, as did a slight excess of LiF (Figure 3c). A 3 M excess of LiF, conversely, resulted in contamination of the sample with LiF, and minor amounts of impurity phases (Figure 3a). However, a 1 M excess amount of LiF as a flux produced an almost pure single-phase $Li_5V(PO_4)_2F_2$ microcrystalline powder (Figure 3b) containing only traces of LiF. The processing temperature of 700 °C was clearly optimum, as shown in Figure 4, which displays XRD patterns of the samples prepared by heating the tubes at temperatures from 600 to 900 °C. As shown in patterns a and b in Figure 4, when the heating temperature was higher than 800 °C, the product was $Li_3V_2(PO_4)_3$, the thermodynamically stable phase. At temperatures less than 600 °C (Figure 4d), it was very difficult to form $Li_5V(PO_4)_2F_2$, and instead a mixture of $Li_5V(PO_4)_2F_2$, Li_3PO_4, V_2O_3, and $Li_3V_2(PO_4)_3$ was formed. Figure 4c again shows the XRD pattern of the sample prepared at 700 °C for comparison, indicating its relative purity.

All the samples all have a minor fraction of LiF as shown in Figure 3b or Figure 4c because of the slight excess used. However, it can be readily extracted in a N-methyl formamide (NMF) solution. The XRD pattern in Figure 5a, together with the Rietveld refinement based on the single-crystal data reported in our previous paper, confirms the sample purity. The diffraction peaks of LiF have completely disappeared, and no second

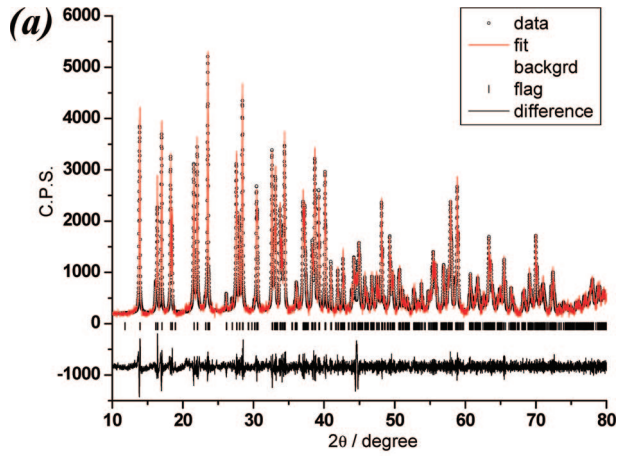

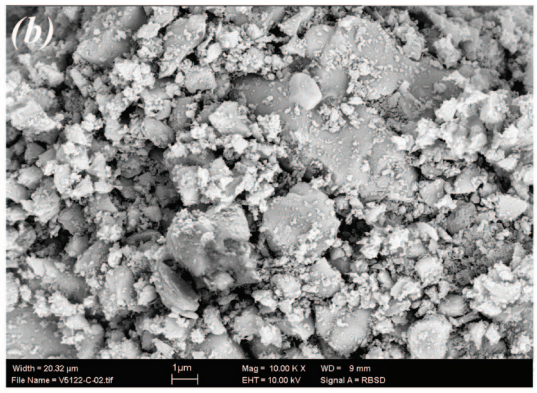

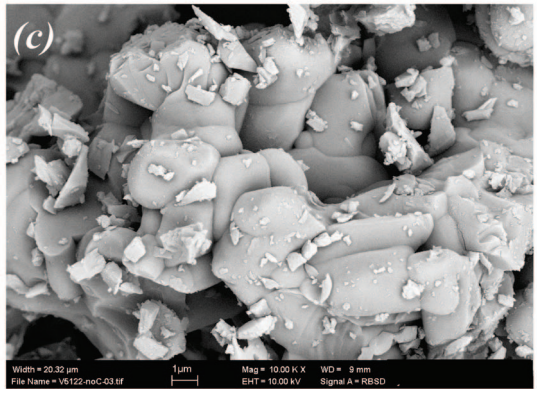

Figure 5. (a) XRD pattern of pure, single-phase $Li_5V(PO_4)_2F_2$ together with the refinement based on a monoclinic lattice having a space group of $P2_1/c$. The experimental (○) and calculated (−) diffraction patterns are shown along with the (*hkl*) reflections (|) and the difference curve. Lattice parameters (virtually identical to those based on our single-crystal structure, in ref 13) and agreement factors are as follows: $a = 6.3646(3)$ Å, $b = 10.8086(8)$ Å, $c = 10.4170(1)$ Å $= 90.000$, $\beta = 90.029(9)°$; wR_p 12.5%, $R_p = 9.0\%$; (b) SEM micrograph of the pure single-phase material prepared using the carbothermal reduction method as described in the text; (c) SEM micrograph of $Li_5V(PO_4)_2F_2$ at the same magnification, prepared in the absence of carbon (see text).

phase is visible. We note that one effect of the carbothermal reduction process is to beneficially reduce the size of the $Li_5V(PO_4)_2F_2$ to about 1−2 μm, as shown in the SEM image of the final pure carbothermal material (Figure 5b). In comparison, the carbon-free material prepared by mixing pure VPO_4 with Li_3PO_4 and a stoichiometric excess of LiF and firing under flowing Ar for 15 min at 700 °C, as described previously,[13] gives rise to crystallites about 2−10 μm in size (Figure 5c). The intimately mixed carbon particles are also clearly visible littering the surface of the carbothermal product. This also

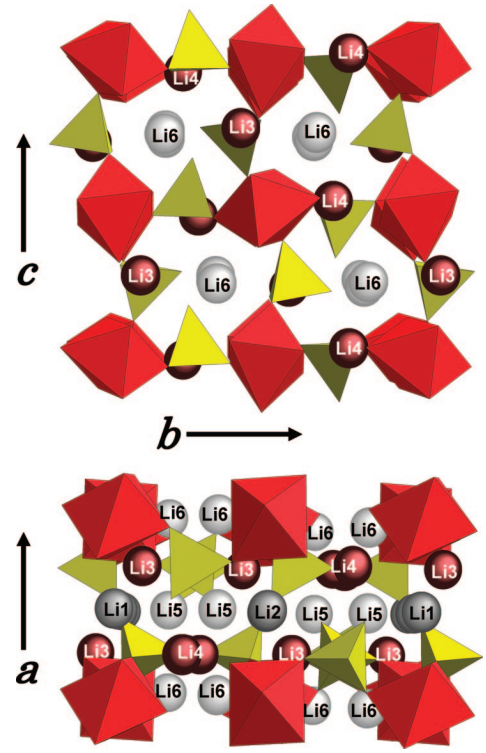

Figure 6. Schematic illustration of the crystal structure of $Li_5V(PO_4)_2F_2$ (space group: $P2_1/c$). $Li_5V(PO_4)_2F_2$ has possible one-dimensional lithium-ion conduction paths along the *a*-axis and two-dimensional paths parallel to the *bc*-plane. The lithium ions are represented according to their bond sun value (bsv): red (highest bsv), light-gray (lowest bsv) and dark-gray (intermediate bsv). The VO_6 octahedra and PO_4 tetrahedra are in red and yellow respectively.

greatly benefits the electrochemistry, although the method necessary for deposition of the carbon does not allow it to smoothly coat the surface.

Electrochemical Behavior of the $Li_5V(PO_4)_2F_2$/C Composite in Lithium Cells. Figure 6 depicts the crystal structure of $Li_5V(PO_4)_2F_2$, which has a layered monoclinic lattice comprised of alternately stacked lithium and vanadium fluorophosphates sheets. Two likely lithium-ion conduction routes are evident in the crystal structure: one is the one-dimensional lithium channels that run along the *a*-axis, and the other is the two-dimensional lithium sheets that lie in the (100) plane. These two paths intersect to form three-dimensional conduction paths. This should lead to facile lithium-ion transport in the structure upon lithium extraction and reinsertion processes. The metal oxide octahedra are interconnected by phosphate groups, giving rise to low intrinsic electronic conductivity of 1.6×10^{-8} S/cm as determined by two-probe dc conductivity measurements. However, this is enhanced in the bulk up to values of 1×10^{-5} S/cm by the 5 wt % carbon content in the composite. Figure 7 shows the charge and discharge curves of $Li_5V(PO_4)_2F_2$ in different voltage windows. There are two plateaus upon charge in the wider voltage window (Figure 7a). The end of the first plateau corresponds to a capacity of about 80−90 mA h g^{-1}, indicating that one lithium ion is extracted, and $Li_5V^{3+}(PO_4)_2F_2$ is oxidized to $Li_4V^{4+}(PO_4)_2F_2$. The capacity is in excellent agreement with the theoretical value of 86 mA h g^{-1}. The average voltage of the first plateau is at 4.15 V, which is almost the same as other V^{3+}/V^{4+} couples at 4.2 V in $LiVPO_4F$ and at 4.1 V in $Li_3V_2(PO_4)_3$, which have similar lattice connectivity.

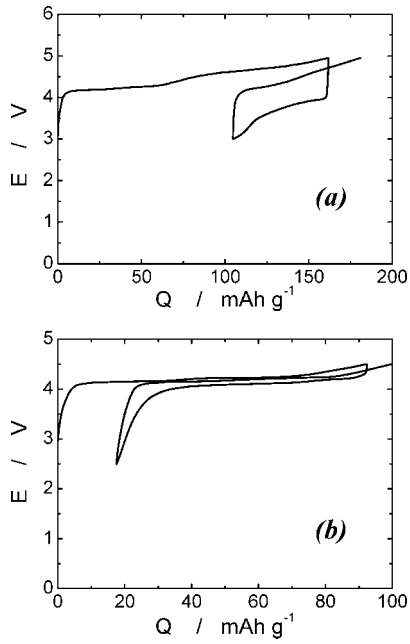

Figure 7. Charge and discharge curves of lithium cells of $Li_5V(PO_4)_2F_2$ operated in voltage windows of (a) 3.0−5.0 V at a rate of *C*/10 or (b) 3.0−4.5 V at *C*/5 at 30 °C. The electrolyte used was 1 M $LiPF_6$ dissolved in EC/DMC (1/1 by volume). The electrode mix consisted of 88 wt % $Li_5V(PO_4)_2F_2$/C, 6 wt % Super S carbon, and 6 wt % PVdF binder.

When the upper voltage window is raised to 5 V, almost two lithium ions are extracted from the solid matrix at 4.65 V to form $Li_3V^{5+}(PO_4)_2F_2$, with a charge capacity of 162 mA h g^{-1} (theoretical capacity = 170 mA h g^{-1}). This potential is proximate to the V^{4+}/V^{5+} couple at 4.6 V in $Li_3V_2(PO_4)_3$. Nonetheless, the second electrochemical process is not reversible as the first, as can be seen in Figure 7a. This is probably the result of structural instability on full charge because of the formation of 100% V^{5+}, which does not favor an octahedral environment. Other factors could also play a role, such as electrolyte oxidation at the higher potential, and partial dissolution of the cathode material. We note that extraction of all three Li from monoclinic $Li_3V_2(PO_4)_3$, in contrast, is more reversible,[11,17] perhaps because a 50:50 mixed oxidation state $V^{4+/5+}$ is formed that stabilizes that structure.

The process corresponding to the first transition to form $Li_4V(PO_4)_2F_2$ is reversible, however, as shown in Figure 7b. The cell possesses a flat operating voltage at 4.15 V with some irreversibility on the first cycle, which we attribute to poor carbon contact, and only a small polarization. We note the latter is quite low despite the relatively large crystallite size and moderate bulk electronic conductivity that we were able to achieve through the carbon deposition method. Thus, the electrochemical data indicate that the $Li_5V(PO_4)_2F_2$/C composite exhibits good kinetics upon lithium extraction and reinsertion as we expect from the crystal structure. This is also suggested by rate studies. Charge−discharge curves for $Li_5V(PO_4)_2F_2$ operated in a voltage window of 2.5−4.5 V, at a rate of either *C*/5 or *C*/30 are further compared in Figure 8. The charge capacity at *C*/5 is only slightly less than at *C*/10. The overall reversible capacity of about 70 mA h g^{-1}

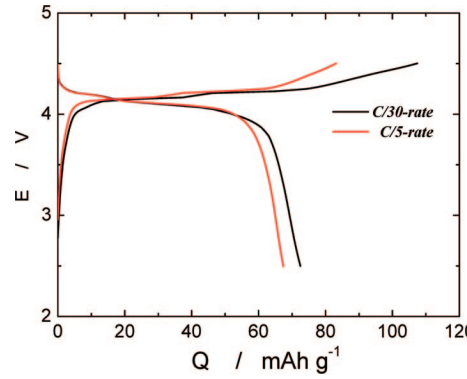

Figure 8. Charge−discharge curves for $Li_5V(PO_4)_2F_2$ operated in a voltage window of 2.5−4.5 V, at a rate of either *C*/30 or *C*/5 at 30 °C. The electrode and cell configuration were the same as described in Figure 7, except that Ketjen black was used as the conductive additive in place of Super S carbon.

at *C*/5 is about the same as that at *C*/10, indicating a rather minor rate dependence. At *C*/30, the discharge capacity is also very similar to *C*/10, but more irreversibility is evident along with "overcharge" on the charge curve, indicating that indeed, electrolyte oxidation and/or dissolution (favored at slower rates) are contributing factors.

The question of the mobility of the lithium ions within the two- or three-dimensional structure next arises. As described in our previous paper,[13] bond sum values (bsv's) for lithium environments in $Li_5V(PO_4)_2F_2$ indicate which lithium ions are the most easily extracted on charge.[18] As shown in Figure 6, lithium ions Li3 and Li4 are more tightly bound from this viewpoint (bsv's between 0.99 and 1.08), whereas the light-gray colored lithium ions are the least tightly bound (Li5 and Li6 with bsv's of about 0.81). They are located at one-dimensional channels along the *a*-axis and at the intersections of the lithium channels and the lithium layers. The dark-gray colored lithium ions are intermediate based on bond sum calculations (Li1 and Li2, with values of 0.96 and 0.88, respectively). In principle, this also defines which lithium ions are the most mobile on the basis of the depth of the potential well (and associated activation energy), but the other consideration for mobility/exchange is the activation energy for the ion to pass through the window between two sites. This is not defined by the bond sum, but by the bottleneck size. Having established the protocol to prepare pure single-phase materials, we therefore turned to ^{6}Li MAS NMR to examine this further, and to investigate Li^+ dynamics.

Solid-State NMR Study. Both natural abundance, and ^{6}Li-substituted $Li_5V(PO_4)_2F_2$ were prepared to investigate the local lithium environments. The ^{7}Li and ^{6}Li MAS NMR spectra are shown in panels a and b in Figure 9. The ^{6}Li acquisition shows much narrower lineshapes (by at least a factor of 5), allowing for resolution of the resonance around 0 ppm. This suggests that the quadrupolar interaction is the primary contributor to the broadening of the resonances, not the paramagnetic interaction, because ^{6}Li has the lower quadrupolar coupling constant. The six crystallographic

(17) (a) Huang, H.; Yin, S.-C.; Kerr, T.; Nazar, L. F. *Adv. Mater.* **2002**, *14* (21), 1525. (b) Saïdi, M. Y.; Barker, J.; Huang, H.; Adamson, G. *Electrochem. Solid-State Lett.* **2002**, *5*, A149.

(18) Yin, S.-C.; Grondey, H.; Strobel, P.; Anne, M.; Nazar, L. F. *J. Am. Chem. Soc.* **2003**, *125*, 10402.

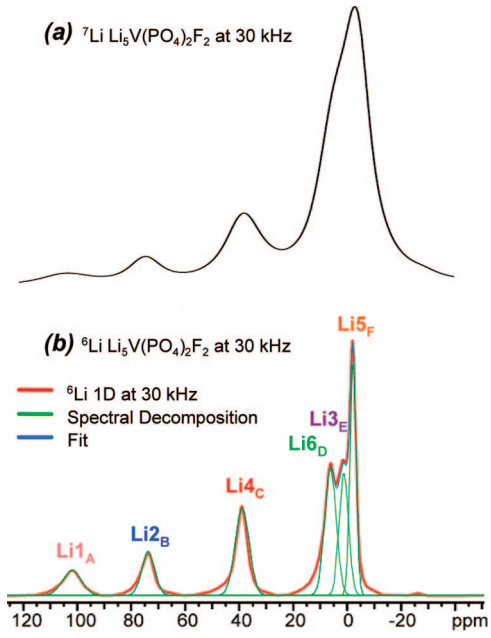

Figure 9. (a) ^{7}Li and (b) ^{6}Li MAS NMR spectra of $Li_5V(PO_4)_2F_2$. The former sample was prepared using natural abundant Li, while the latter was substituted ca. 60% by ^{6}Li. Note that (b) also includes the results of spectral deconvolution. The peaks are labeled $Li\alpha_\beta$ where α is the crystallographic site number and β is the resonance (from highest to lowest frequency). We note that the very weak signal visible at −25 ppm arises from the background in this probe.

Table 1. Local Environments for the Six Unique Li Sites as Defined by the Values of Li−O−V angles, Li−F−V Angles, and Li−V Bond Lengths

Li site	Li−O−V angle (deg)	Li−F−V angle (deg)	Li−V distance (Å)
1	102		3.18
	102		3.18
		97	3.18
		97	3.18
2	101		3.18
	101		3.18
		94	3.18
		94	3.18
3	93		3.03
	97		3.03
		120	3.39
		75	3.03
4	93		2.92
	86		2.92
		83	2.92
		123	3.40
5		140	4.56
		151	4.34
6	94		3.17
	99		3.13
		96	3.17
		93	3.13

lithium sites can be resolved in the ^{6}Li spectrum by deconvolution, and are labeled A−F from highest to lowest frequency.

The large chemical shifts observed, particularly for peaks A−C, result from the well-known Fermi-contact mechanism that is based on transfer of unpaired electron density from the paramagnetic V^{3+} centers to the lithium nuclei. There are two types of interaction, delocalization and polarization. As the electron configuration of the d-electrons here is $t_{2g}^2e_g^0$, the possible transfer mechanisms here are a 90° delocalization, in which the occupied t_{2g} donates positive electron density to the lithium orbital via direct overlap of the orbitals, or a 180° polarization transfer, in which the occupied t_{2g} polarizes the e_g, and transfers negative electron density to the lithium center.[19] Delocalization has a larger contribution due to the direct overlap of orbitals of the correct symmetry, giving rise to chemical shifts of higher frequency. The closer the angle to a 90° interaction, the more extensive the delocalization mechanism. Thus, depending on the angle of the interaction and bond length, either high or low chemical shifts can result. In this case, there are no 180° bonding interactions between Li−O(F)−V, and thus the polarization mechanism is neglected in the assignment below.

The magnitude of the Fermi-contact interaction is additive and depends on the number of d electrons (two for V^{3+} in this case) and the Li−O(F)-V bond angles and distances. Only the vanadium atoms in the immediate local environment of the lithium, listed in Table 1, are able to donate electron density. Note that five of the six lithium local environments have two different vanadium centers that donate electron density via a total of four pathways: using two oxygen and two fluorine atoms. Li5 also receives electron density from two vanadium centers but this only occurs through two pathways via fluorine atoms. Therefore, attempting to assign resonances to specific Li sites can be very complex, even more so than for lithium manganates where an elegant study has been reported.[20]

Table 1 summarizes the local environments of the six Li sites, determined from single-crystal X-ray diffraction results.[13] Comparing the areas of the resonances in the ^{6}Li spectral decomposition in Figure 9b, we see that the relative intensity ratio is 0.5:0.5:1:1:1:1 for resonances A−F respectively. According to the site occupancy determined by XRD, resonances A and B must correspond to Li1 and Li2. These are Li ions that sit on the half-occupied 2b and 2d special sites in the structure based on the $P2_1/c$ space group.[13] They can be distinguished in the NMR spectrum by considering the local environments of the two sites. The local coordination to the vanadium centers is virtually identical and cannot account for the large difference in chemical shift (Figure 6). However, the two Li sites have large differences in site volume. Li2 has longer contacts to the nearest neighboring oxygen atoms, giving it a larger site volume (and a much lower bond sum value of 0.88 compared to 0.96 for Li1). We propose that this difference, together with the inherent mobility of the lithium ions in their sites, results in a lower net overlap of the Li−V orbitals and thus a lower chemical shift for the site of larger volume. Therefore, we assign Li1 to resonance A, and Li2 to resonance B.

Li4 has the shortest Li−V distances and both Li−O−V angles are close to 90°. It also has a short Li−V distance via a Li−F−V pathway. As both factors favor the delocalization mechanism, this site would be expected to have a resonance at the next highest frequency, resonance C. It is surprising that Li4's shift of 39 ppm is lower than that observed for $Li1_A$ and Li_B, even though the Li−V distances are shorter, and the bond sum calculation is

(19) Carlier, D.; Menetrier, M.; Grey, C. P.; Delmas, C.; Ceder, G. *Phys. Rev. B: Condens. Matter Mater.Phys.* **2003**, *67*, 174103/1.
(20) Lee, Y. L.; Wang, F.; Grey, C. P. *J. Am. Chem. Soc.* **1998**, *120*, 12601.

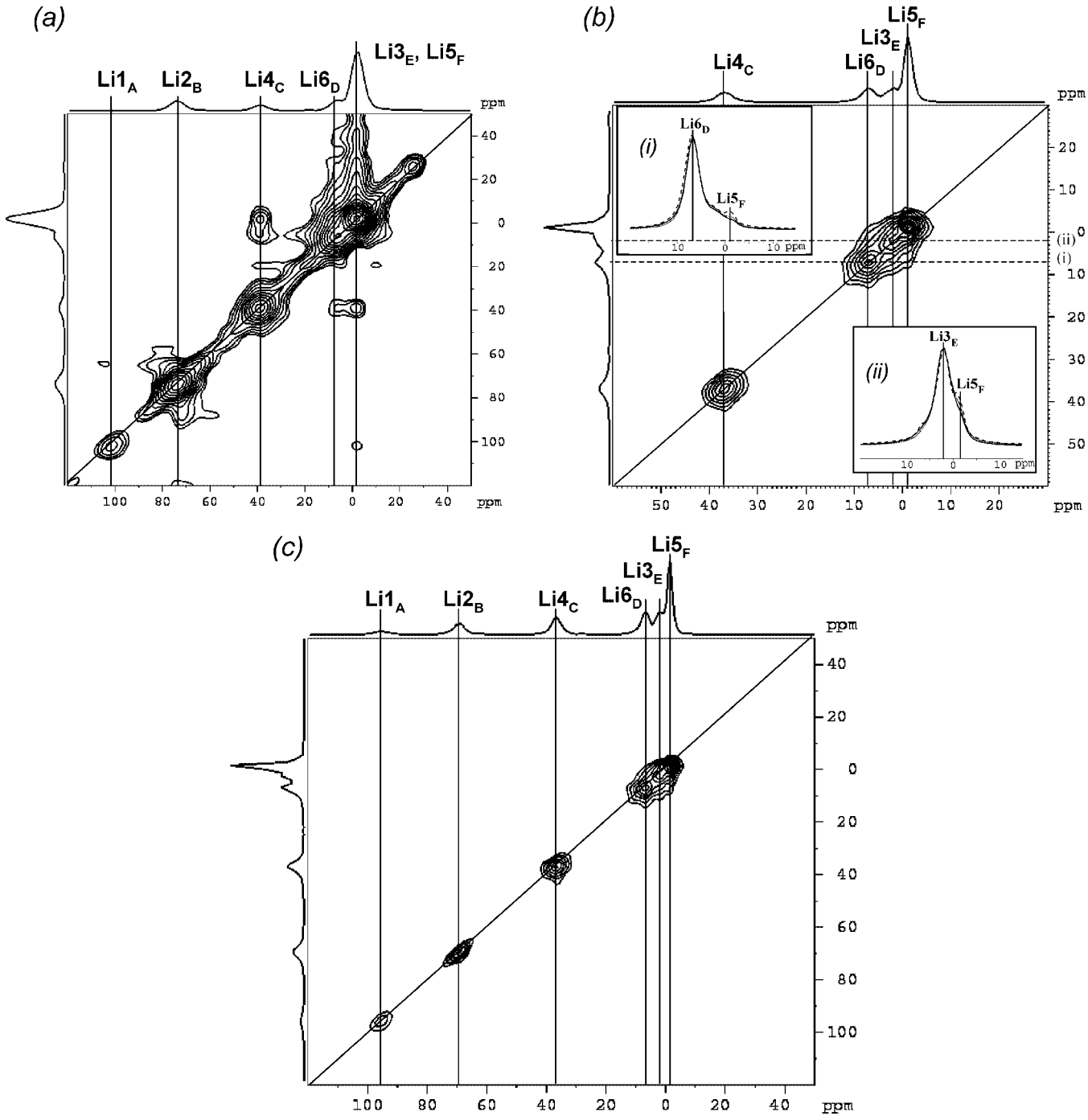

Figure 10. ^{7}Li 2D EXSY spectrum for $Li_5V(PO_4)_2F_2$ at 40 kHz with mixing times (a) 7 ms, (b) 1 ms, and (c) 1 μs. The 1D projections are shown. The insets (i) and (ii) represent slices from 6 and 2 ppm, respectively (shown as the dashed line on the spectrum), taken from the series of three data sets with mixing times of 1 ms (dashed line), 500 μs (dotted line), and 1 μs (solid line).

larger. However, the assignment is unequivocal, on the basis of the signal intensities, which are convincingly different for the fully occupied versus 1/2 occupied sites. It is also confirmed by the 2D spectra discussed below. Careful examination of the structural details in Table 1 highlights the subtleties of making such assignments. Li5 is assigned to resonance F because it has Li−F−V bond angles that deviate substantially from 90°, and long Li−V distances (Table 1). Both factors contribute to the comparatively small chemical shift of −2 ppm. The bond angles intermediate between 90° and 180° results in poor overlap for electron transfer via the delocalization mechanism. Thus, the only NMR signals that remain to be assigned are resonances D and E. A more detailed investigation using two-dimensional spectroscopy was necessary to distinguish between these.

Two-dimensional exchange spectroscopy (EXSY) is used to study chemical exchange among multiple sites.[21] The direct exchange of lithium sites can be observed as cross peaks in the spectra. Figure 10 shows 2D EXSY spectra at 300K for $Li_5V(PO_4)_2F_2$, for three different mixing time scales

(21) Jeener, J.; Meier, B. H.; Bachmann, P.; Ernst, R. R. *J. Chem. Phys.* **1979**, *71*, 4546.

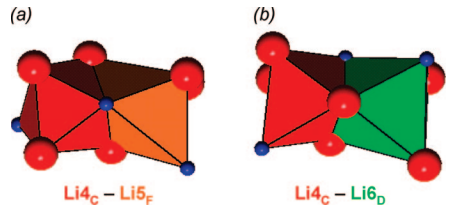

Figure 11. Li local environments represented as polyhedra for $Li4_C$ (red), $Li5_F$ (orange), and $Li6_D$ (green). The direct pathways for exchange are shown (a) between $Li4_C$ and $Li5_F$ (Li−Li distance of 2.74(9) Å) and (b) between $Li4_C$ and $Li6_D$ (Li−Li distance of 2.83(0) Å). Oxygen atoms and fluorine atoms are shown in red and blue, respectively.

Table 2. Assignment of the Li Chemical Shifts to the Crystallographic Sites

chemical shift (ppm)	Li resonance	Li site
102	A	1
74	B	2
39	C	4
6	D	6
1	E	3
−2	F	5

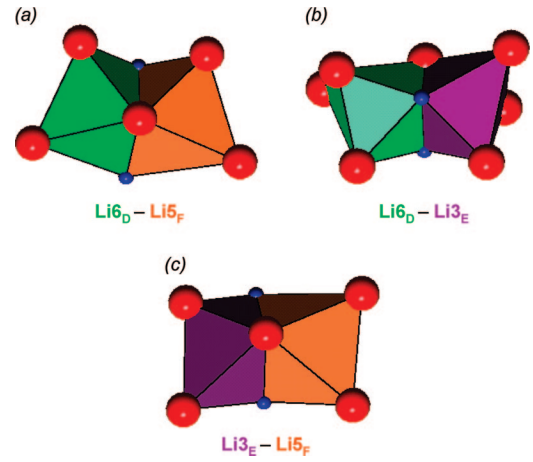

Figure 12. Li local environments represented as polyhedra for $Li3_E$ (purple), $Li5_F$ (orange), and $Li6_D$ (green). The direct pathways for exchange are shown (a) between $Li6_D$ and $Li5_F$ (Li−Li distance of 3.02(6) Å), (b) between $Li6_D$ and $Li3_E$ (Li−Li distance of 3.30(1) Å), and (c) between $Li3_E$ and $Li5_F$ (Li−Li distance of 3.09(4) Å). Oxygen atoms and fluorine atoms are shown in red and blue, respectively.

of 7 ms, 1 ms and 1 μs. The upper limit was chosen on the basis of the spin−lattice relaxation time; the intermediate value is the minimum time needed for the onset of exchange. For comparison, at a mixing time of 1 μs, there is only signal intensity along the diagonal, which indicates no exchange is taking place. The diagonal resonance at −25 ppm arises from background in the probe. Its intensity is subject to broadening processes, and in particular, it becomes visible in Figure 10a, where processing conditions are chosen to highlight the intensity of the cross peaks. Chemical exchange involving $Li1_A$ and $Li2_B$ is not observed up to a mixing time of 7 ms, in accord with their location in the lattice. The sites which clearly exchange on the longer time scale of 7 ms are D−$Li4_C$, $Li4_C$−$Li5_F$, and D−$Li5_F$.[22] $Li4_C$ and Li3 are greater than 4 Å apart and do not have a direct path for interaction. However, $Li4_C$ has a facile pathway for exchange with $Li5_F$ (previously assigned) and Li6 (still unassigned), because each pair shares a triangular face (Figure 11). Because $Li4_C$ does exchange with resonance D, this means that site D must be Li6. This leaves site E as Li3. Table 2 summarizes the full assignment of the six crystallographic sites with the six Li chemical shifts.

Dynamic information on the site exchange was also obtained at faster mixing times, allowing us to more precisely correlate the NMR data with the structural features, and corroborate the assignments given above. At a fast time scale of 1 ms, (Figure 10b) far fewer sites are exchanging. Only the low-frequency quadrant of the spectrum shows any evidence of exchange. The off diagonal intensity, though it overlaps with the diagonal resonances, clearly indicates exchange between sites $Li3_E$−$Li5_F$ and $Li6_D$−$Li5_F$ at 1 ms. This is highlighted using the inset slices extracted at (i) 6 and (ii) 2 ppm in the indirect dimension, which clearly show both the diagonal and off-diagonal resonances. This is emphasized by comparing to slices from the 1 μs mixing time, where only resonances from the diagonal are observed. Slices from a mixing time of 500 μs are also included to demonstrate the initial onset of exchange between sites $Li6_D$−$Li5_F$. It is clear that $Li6_D$ and $Li5_F$ appear to be the most mobile ions in the lattice, in accord with the bond sum calculations (vide supra).

As mentioned earlier, the ease of exchange is not only determined by the depth of the potential well in which the ions rest, but also by the connectivity between the sites. The exchange processes in the lattice can be explained by consideration of these factors. For example, Li1 and Li2 do not possess a direct pathway for exchange and hence there are no cross peaks in the 2D spectra. In order for Li2 and Li5 to exchange, a high-energy interstitial site would have to be occupied adjacent to a P^{5+} ion.[23,24] Treating the Li local environments as polyhedra, it is evident that sites which **do** exchange, namely, $Li4_C$−$Li6_D$, $Li4_C$−$Li5_F$, $Li6_D$−$Li5_F$, $Li6_D$−$Li3_E$, and $Li3_E$−$Li5_F$ all share a face (the latter three pairs are depicted in Figure 12). Closer examination of these pathways reveals that the triangular face shared by the $Li6_D$−$Li5_F$ octahedra is the largest (area of 4.0 $Å^2$), followed by the shared faces of $Li3_E$−$Li5_F$ (area of 3.9 $Å^2$), then $Li4_C$−$Li6_D$ (area of 3.8 $Å^2$) and finally $Li4_C$−$Li5_F$ (area of 3.6 $Å^2$). This may explain why $Li6_D$− $Li5_F$ starts to exchange at the short 500 μs time scale, and exchange involving $Li3_E$ and $Li5_F$ is observed next. Thus exchange along the channels that run along the *a*-axis (Figure 6) and which contain $Li6_D$ and $Li5_F$ dominates the process. On the basis of this set of exchange partners, the diffusion is not strictly one-dimensional, as diffusion between channels (for example $Li4_C$−$Li6_D$, or $Li3_E$−$Li5_F$) is also expected.

The 2D EXSY data determines a millisecond time scale for Li ion motion of sites that exchange in $Li_5V(PO_4)_2F_2$. This result is slower than observed for $Li_3V_2(PO_4)_3$, which exchanges on a microsecond time scale at room tempera-

(22) Note that D-E and E-$Li5_F$ also exchange, but this is only visible by looking at the slices in the indirect dimension of the 2D spectra.

(23) Maldonado-Manso, P.; Losilla, E. R.; Martinez-Lara, M.; Aranda, M. A. G.; Bruque, S.; Mouahid, F. E.; Zahir, M. *Chem. Mater.* **2003**, *15*, 1879.
(24) Cahill, L. S.; Chapman, R. P.; Britten, J. F.; Goward, G. R. *J. Phys. Chem. B* **2006**, *110*, 7171.

ture.[24] The explanation for the slower ion dynamics in $Li_5V(PO_4)_2F_2$ are again based on structural considerations. In the "323" compound, there are vacancies between the Li sites that allow for rapid exchange to take place, whereas in the layered "5122" material, the sites are relatively full and thus prohibit ready exchange. In accord, our preliminary ^{6}Li 2D EXSY results for $Li_4V(PO_4)_2F_2$ prepared by chemical oxidation of $Li_5V(PO_4)_2F_2$ ("4122") confirm a microsecond time scale for Li ion mobility. This suggests that although Li ion mobility is slow in the parent compound, $Li_{5-x}V(PO_4)_2F_2$ displays excellent Li ion diffusion as expected.

Conclusions

Preparation conditions of metastable $Li_5V(PO_4)_2F_2$ were successfully optimized by using an amorphous VPO_4/C composite with large specific surface area, which is key to induce rapid reaction. In addition, rapid heating and quenching using an appropriate flux volume was indispensable for producing a single-phase microcrystalline material. The resultant composite exhibited two plateaus at 4.15 and 4.65 V upon electrochemical lithium extraction process, which are assigned to the redox couples of V^{3+}/V^{4+} and V^{4+}/V^{5+} in the active material, respectively. The first plateau at 4.15 V was reversible with high-rate charge and discharge ability. On the other hand, the second process at 4.65 V was poorly reversible, which is ascribed to the thermodynamically unstable occupancy of V^{5+} in an octahedral site and resultant structural instability.

The ^{6}Li NMR study successfully identified the six crystallographic lithium sites in $Li_5V(PO_4)_2F_2$, and moreover provided a measurement of dynamic exchange of the lithium ions. Of the two possible pathways for conduction, the 2D EXSY results confirm that Li ions exchange along the *a*-axis but, surprisingly, not through the lithium layers that lie in the (100) plane. Such site-specific information about exchange processes is uniquely available through solid-state NMR studies of this kind. The two-dimensional lattice of the fully "stuffed" $Li_5V(PO_4)_2F_2$ is not conducive to rapid lithium exchange, probably because of the high degree of ordering of the Li sites and lack of vacancies, as observed previously for $Na_5Al(PO_4)_2F_2$.[25] Partial lithium extraction, however, increases the lithium mobility by a factor of 1×10^3, which will be reported more fully in a subsequent paper.

Acknowledgment. L.F.N. and G.G. thank NSERC and MMO/EMK for financial assistance. L.S.C. acknowledges support through the NSERC PGS-D program. Y.I. is grateful to Kyoto University, Japan, for sabbatical travel funds.

CM702346N

(25) Poojary, D. M. Clearfield, A., Timofeeva, V. A., Sigaryov, S. E. *Solid State Ionics* **1994**, *73*, 75.